

The first photometric investigations of the G-type shallow contact binary IO Cnc

Wen-Ping Liao (廖文萍)^{1,2,3,4}, Lin-Jia Li (李临甲)^{1,2,3}, Xiao Zhou (周肖)^{1,2,3} and Qi-Shan Wang (王琪善)^{1,4}

¹ Yunnan Observatories, Chinese Academy of Sciences, Kunming 650216, China; liaoowp@ynao.ac.cn

² Key Laboratory for the Structure and Evolution of Celestial Objects, Chinese Academy of Sciences, Kunming 650216, China

³ Center for Astronomical Mega-Science, Chinese Academy of Sciences, Beijing 100101, China

⁴ University of Chinese Academy of Sciences, Beijing 100049, China

Received 2020 June 12; accepted 2020 August 13

Abstract IO Cnc was classified to be a new G-type (G0) W UMa-type eclipsing binary system. Our first multicolor photometric solutions show that IO Cnc is a new W-subtype shallow contact binary with a fill-out factor of $f = 16.1\%$ and a low mass ratio of $q = 3.12$ (or $1/q = 0.32$). During orbital period investigations, a cyclic variation and a downward parabolic variation with a rate of $(-1.28 \pm 0.43) \times 10^{-7} \text{ d yr}^{-1}$ was discovered in the observed–calculated ($O - C$) curve. The cyclic variation was analyzed by the light travel time effect (LTTE) via a potential red dwarf companion star, an orbital semi-major axis shorter than $4.88 \pm 0.82 \text{ AU}$ was obtained. Finally, we collect physical parameters of a sample of 50 G-type shallow contact binaries ($f \leq 20\%$), it is suggested that most of the G-type shallow contact binaries are undergoing a long-term and periodic orbital period changes, especially more systems show long-term decreases. The long-term orbital period decrease indicates that IO Cnc is in a mass transferring from the more massive component to the less massive one. With the long-term decrease of the orbital period, this shallow contact binary will evolve into a deeper contact one.

Key words: stars: binaries: close — stars: binaries: eclipsing — stars: individual (IO Cnc) — stars: solar-type — stars: evolution

1 INTRODUCTION

Contact binaries (i.e., W UMa type binaries) usually consist of two late-type components. Both components fill their critical Roche lobes, and sharing a common convective envelope (CCE). Contact binaries have the shortest periods and the lowest angular momentums among main-sequence binaries. Statistical studies have shown that most contact binaries are solar-type main-sequence stars (Wang et al. 2020). The solar-type contact binaries are the key observing samples, which may provide some similarity to our Sun, such as magnetic activity, oscillation and so on. In addition, it is very important to study the correlation amongst physical parameters for the solar-type binaries. The long-term monitoring on solar-type contact binaries are helpful for understanding the magnetic activities and evolutions of solar-like stars in extreme physical conditions (fast rotation, common convective envelop, etc.) (Wang et al. 2017). Moreover, more and more evidence

shows that many contact binaries are located in multiple star systems (e.g., Liao & Sarotsakulchai 2019; Liao et al. 2019; Shi et al. 2020; Wang et al. 2020; Zhang et al. 2020; Zhou & Soonthornthum 2020). Study on the contact binaries in multiple star systems, which could provide a lot of information for the formation and evolution of contact binaries, should be a potential growing point for understanding the contact binaries' evolution. In this study, we presented the orbital period changes and evolutionary status for the solar-type contact binary IO Cnc.

The object IO Cnc (= GSC 01402–00052) is a short-period binary system with an orbital period of 0.347694 days. It was discovered in 2003 (Rinner et al. 2003), where it was classified as a new W UMa variable, and its light variation amplitude is $0^{\text{m}}.576 \pm 0^{\text{m}}.023$. After its discovery, only some times of light minima were reported. Neither photometric solutions nor orbital period analyses for this system have been published.

Based on the released data of the Large Sky Area Multi-Object Fiber Spectroscopic Telescope (LAMOST), physical properties and a catalog of EW-type eclipsing binaries were given by Qian et al. (2017). During 2013, IO Cnc was observed by LAMOST three times. The spectral parameters of this binary were given. According to the distribution of the gravitational acceleration ($\log(g)$) and metallicity ($[\text{Fe}/\text{H}]$) for EWs (Qian et al. 2017), the values of $\log(g)$ and $[\text{Fe}/\text{H}]$ for IO Cnc are near the peak, indicating that it belongs to a typical EW-type eclipsing binary.

In the present paper, multi-band CCD light curves and orbital period variations of IO Cnc are firstly investigated. Then, combing statistics of 50 G-type shallow contact binaries, the configuration and evolutionary state, physical parameters of multiple star system are discussed.

2 NEW CCD PHOTOMETRY

From January 2014 to May 2018 (between HJD 2456659 and HJD 2458243), CCD observations of IO Cnc were carried out with those three telescopes in China, i.e., the 85 cm reflecting telescope at the Xinglong Station of National Astronomical Observatories, Chinese Academy of Sciences (NAOC), which was equipped with PI1024 BFT 1024×1024 CCD (Back-illuminated, Frame-Transfer CCD); the 1.0 m and 60 cm Cassegrain reflecting telescopes equipped with Andor DW436 2048×2048 CCD at Yunnan Observatories (YNOs). The observation log is given in Table 1. Bias and flat-field images were also taken on all the observing nights for use in preprocessing.

All the CCD images were processed with the DAOPHOT package of IRAF in a standard mode to determine differential magnitudes. A set of complete light curves and nine new minimum curves were obtained. During light curve observations, the exposure times for $V(RI)c$ bands were set as 40 s, 30 s, and 20 s, respectively. In order to get better light curves of IO Cnc, the fluxes of four stars in the field were summed together into one comparison star, and their differential magnitudes were determined to verify that the four comparison stars are invariable. The coordinates and magnitudes of the variable and comparison stars are tabulated in Table 2. The phased light curves calculated with Equation (1) are displayed in Figure 1. Heliocentric Julian dates (JD (Hel.)) and the differential magnitudes ($\Delta(m)$) are given in Table 3. As shown in Figure 1, the light curves are typical EW-type with a small difference in the depths of the primary and secondary. Nine new times of light minima determined with our observations are listed in Table 4.

Table 1 Observation Log

Date	Filters	Telescopes	Type
2014 Jan 01	VR_cI_c	85 cm	light curve
2014 Jan 07	VR_cI_c	85 cm	light curve
2014 Jan 11	R_cI_c	1 m	minimum light
2014 Mar 17	N	1 m	minimum light
2015 Mar 05	N	60 cm	minimum light
2016 Jan 15	N	60 cm	minimum light
2016 Nov 12	I_c	60 cm	minimum light
2017 Apr 08	R_cI_c	60 cm	minimum light
2018 May 04	R_cI_c	60 cm	minimum light

Table 2 Coordinates and Magnitudes of the Variable and Comparison Stars

Targets	$\alpha_{2000.0}$	$\delta_{2000.0}$	Mag.
IO Cnc	09 ^h 17 ^m 16 ^s .08	+16°19′34″.5	$V = 14.44$
Comparison 1	09 ^h 17 ^m 28 ^s .66	+16°22′36″.5	$R = 12.9$
Comparison 2	09 ^h 17 ^m 37 ^s .55	+16°22′06″.8	$R = 13.6$
Comparison 3	09 ^h 17 ^m 25 ^s .74	+16°18′59″.8	$R = 14.8$
Comparison 4	09 ^h 17 ^m 21 ^s .31	+16°17′36″.3	$R = 13.7$

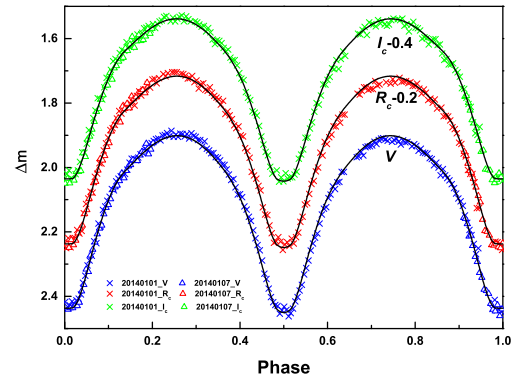


Fig. 1 Observed and theoretical light curves (in black solid lines).

3 THE FIRST PHOTOMETRIC SOLUTIONS BY W-D PROGRAM

To obtain photometric solutions of IO Cnc, the W-D 2013 program (Van Hamme & Wilson 2007; Wilson & Devinney 1971; Wilson 2012) was used to analyze VR_cI_c light curves of the binary system. During the calculation, the mean temperature of 5848 ± 38 K for Star 2 was adopted. For the common convective envelope of both component stars, the gravity-darkening and the bolometric albedos coefficients were fixed to be $g_{1,2} = 0.32$ and $A_{1,2} = 0.5$. The bolometric and bandpass limb-darkening coefficients were obtained by using an internal computation with the logarithmic law.

Firstly, we should obtain initial input values of those parameters (i.e., the mass ratio, q , the orbital inclination,

Table 3 Light Curve Observations for Eclipsing Binary IO Cnc

V-Band							
JD (Hel.)	$\Delta(m)$	JD (Hel.)	$\Delta(m)$	JD (Hel.)	$\Delta(m)$	JD (Hel.)	$\Delta(m)$
2456659.1067	2.439	2456659.1120	2.440	2456659.1173	2.432	2456659.1225	2.425
2456659.1085	2.411	2456659.1138	2.448	2456659.1190	2.428	2456659.1243	2.412
2456659.1103	2.444	2456659.1155	2.417	2456659.1208	2.416	2456659.1260	2.407
.....							
<i>R_c</i> -Band							
JD (Hel.)	$\Delta(m)$	JD (Hel.)	$\Delta(m)$	JD (Hel.)	$\Delta(m)$	JD (Hel.)	$\Delta(m)$
2456659.1074	2.432	2456659.1126	2.436	2456659.1179	2.419	2456659.1232	2.419
2456659.1091	2.430	2456659.1144	2.456	2456659.1196	2.448	2456659.1249	2.394
2456659.1109	2.432	2456659.1161	2.450	2456659.1214	2.419	2456659.1267	2.405
.....							
<i>I_c</i> -Band							
JD (Hel.)	$\Delta(m)$	JD (Hel.)	$\Delta(m)$	JD (Hel.)	$\Delta(m)$	JD (Hel.)	$\Delta(m)$
2456659.1079	2.428	2456659.1131	2.429	2456659.1184	2.409	2456659.1237	2.421
2456659.1096	2.444	2456659.1149	2.442	2456659.1201	2.433	2456659.1254	2.409
2456659.1114	2.429	2456659.1166	2.420	2456659.1219	2.437	2456659.1272	2.383
.....							

This table is available in its entirety in machine-readable and Virtual Observatory (VO) forms in the online journal. The entire table is available at <http://www.raa-journal.org/docs/Supp/ms4702Table3.txt>. A portion is shown here for guidance regarding its form and content.

i , the mean temperature of Star 1, T_1 , the monochromatic luminosity of Star 1, L_1 , and the dimensionless surface potential $\Omega_1 = \Omega_2$ for contact mode), therefore, a well-known q -search method was used. We assumed a series of trial values of q during the q -search process. The q -search diagram was plotted in the left panel of Figure 2. It is shown that the minimum value of mean residual Σ is achieved at $q = 3.1$. The final basic photometric solutions (without spot or third light) were obtained by performing a series of differential corrections, which are listed in Column (2) of Table 5. Theoretical light curves (black lines) calculated with basic photometric solutions compared with the normal points of the observed light curves (color points) are shown in Figure 1. The corresponding fitting residuals are displayed in the right panel of Figure 2. The basic photometric solutions show that IO Cnc is a newly discovered W-subtype shallow contact binary with a mass ratio of $q = 3.120 \pm 0.025$ and a fill-out factor of $f = 16.1\% \pm 5.0\%$.

4 ORBITAL PERIOD VARIATIONS

To investigate the orbital period variations, all available times of light minima are tabulated in Table 4, where 15 new times of light minima of CRTS project data¹ (Drake et al. 2009) obtained by using the method of Li & Qian (2014) and Li et al. (2018a) are listed. The eclipse time, HJD 2451491.656 from ROTSE survey was not used because of its low precision. The $(O - C)_1$ values are computed with the following linear ephemeris, where 2456665.37344 is one of the times of light minima obtained with our observations and a period of 0.347694

days from $O - C$ gateway website was assumed.

$$\text{Min}I = 2456665.37344(34) + 0^d.347694 \times E. \quad (1)$$

The corresponding $(O - C)_1$ curves are displayed in the upper panel of Figure 3 along with the epoch number, E , where green and red dots represent new observations in the present paper and times of light minima obtained from the CRTS project data, respectively.

From the $(O - C)_1$ diagram of IO Cnc, a cyclic oscillation superimposed on a continuous period change exists. In the process of analysis, we have tried to consider a general case of an eccentric orbit. However, no credible results were obtained because: 1) the parameter errors obtained are several times of the parameters themselves; 2) or the period P_3 obtained is longer than the data duration. Therefore, we tried to use a pattern of parabolic-plus-pure cyclic variation to fit the trend of the $(O - C)_1$ changes. A weight of $1/\sigma^2$ was applied to observations during the analysis. Then, based on a weighted least-squares method, the $(O - C)_1$ diagram of IO Cnc was fitted by the following equation,

$$O - C = \Delta JD_0 + \Delta P_0 E + \frac{\beta}{2} E^2 + A \sin(\Omega_1 E + \varphi), \quad (2)$$

where $\Omega_1 = 360^\circ P/P_3$ (P is the orbital period of eclipsing binary, P_3 is the orbital period of the third body). The fitting parameters of orbital period variations are listed in the upper part of Table 6.

The upper panel of Figure 3 is the fitting result, while cyclic variations caused by the third body are easily seen from the middle panel. The residuals are shown in the lower panel, where no apparent regularity can be traced.

¹ <http://crts.caltech.edu/>

Table 4 All Available Times of Light Minima for IO Cnc

HJD	Errors (σ) (d)	Min.	E	$(O - C)_1$ (d)	$(O - C)_2$ (d)	Ref.
2452721.4882	0.0019	p	-11343	0.0078	-0.0036	[1]
2453855.84494	0.00076	s	-8080.5	0.0129	0.0021	CRTS
2454124.95962	0.00064	s	-7306.5	0.0124	0.0020	CRTS
2454148.42876	0.00082	p	-7239	0.0122	-0.0018	CRTS
2454474.91551	0.00093	p	-6300	0.0143	0.0045	CRTS
2454494.03729	0.00067	p	-6245	0.0129	0.0031	CRTS
2454848.8582	0.0006	s	-5224.5	0.0121	0.0030	[2]
2454849.9018	0.0004	s	-5221.5	0.0126	0.0035	[2]
2454853.55175	0.00068	p	-5211	0.0117	0.0027	CRTS
2454855.46616	0.00110	s	-5205.5	0.0138	0.0048	CRTS
2455195.50662	0.00097	s	-4227.5	0.0096	0.0013	CRTS
2455205.9378	0.0002	s	-4197.5	0.0099	0.0017	[3]
2455231.49329	0.00074	p	-4124	0.0099	0.0018	CRTS
2455295.4652	0.0022	p	-3940	0.0061	-0.0019	[4]
2455577.9670	0.0007	s	-3127.5	0.0065	-0.0007	[5]
2455591.52842	0.00078	s	-3088.5	0.0079	0.0007	CRTS
2455593.61281	0.00097	s	-3082.5	0.0061	-0.0010	CRTS
2455625.4271	0.0027	p	-2991	0.0064	-0.0007	[6]
2455625.6003	0.0023	s	-2990.5	0.0058	-0.0013	[6]
2455629.4260	0.0003	s	-2979.5	0.0068	-0.0002	[7]
2455649.4166	0.0003	p	-2922	0.0050	-0.0020	[7]
2455663.6733	0.0006	p	-2881	0.0063	-0.0006	[5]
2455940.08856	0.00075	p	-2086	0.0048	-0.0013	CRTS
2455963.5555	0.0008	s	-2018.5	0.0024	-0.0036	[7]
2455974.68132	0.00110	s	-1986.5	0.0020	-0.0040	CRTS
2456003.7142	0.0004	p	-1903	0.0024	-0.0035	[8]
2456010.4972	0.0008	s	-1883.5	0.0054	-0.0004	[7]
2456224.84858	0.00087	p	-1267	0.0034	-0.0017	CRTS
2456265.69480	0.00166	s	-1149.5	-0.0044	-0.0093	CRTS
2456309.8611	0.0005	s	-1022.5	0.0048	0.0000	[9]
2456659.28955	0.00032	s	-17.5	0.0008	-0.0027	This study
2456665.37344	0.00034	p	0	0.0000	-0.0034	This study
2456669.19770	0.00021	p	11	-0.0004	-0.0038	This study
2456734.04301	0.00069	s	197.5	0.0000	-0.0031	This study
2456747.4258	0.0009	p	236	-0.0034	-0.0065	[10]
2456765.3354	0.0003	s	287.5	-0.0001	-0.0031	[10]
2457074.4373	0.0016	s	1176.5	0.0019	0.0002	[11]
2457074.6089	0.0008	p	1177	-0.0004	-0.0021	[11]
2457087.12734	0.00099	p	1213	0.0011	-0.0005	This study
2457105.3836	0.0008	s	1265.5	0.0034	0.0018	[12]
2457403.35454	0.00042	s	2122.5	0.0006	0.0004	This study
2457705.32696	0.00038	p	2991	0.0008	0.0021	This study
2457852.05287	0.00033	p	3413	-0.0002	0.0019	This study
2458243.03471	0.00044	s	4537.5	-0.0003	0.0039	This study

References: [1] Rinner et al. (2003); [2] Diethelm (2009); [3] Diethelm (2010); [4] Hubscher & Moninger (2011); [5] Diethelm (2011); [6] Hubscher et al. (2012); [7] Hoňková et al. (2013); [8] Diethelm (2012); [9] Diethelm (2013); [10] Hoňková et al. (2015); [11] Hubscher (2015); [12] Juryšek et al. (2017).

5 DISCUSSIONS AND CONCLUSIONS

The light curves for totally eclipsing G-type binary IO Cnc were analysed with W–D method. It is found that it is a new W-subtype shallow contact binary with much more massive but cooler component ($q \simeq 3.120$, $T_2/T_1 \simeq 0.98$ and $f = 16.1 \pm 5.0\%$). The photometric results are reliable for such contact binaries having total eclipses (Terrell & Wilson 2005; Li et al. 2018b; Liao et al. 2019). The mass of the more massive component can be estimated with mean spectroscopic type of G0 for IO Cnc $\sim 1.05 M_\odot$. Then, the mass of the less massive component is determined to be $M_1 = 0.34 \pm 0.01 M_\odot$. With the same method as Liao et al. (2013) used, the absolute parameters

of IO Cnc are determined as $R_1 = 0.69 \pm 0.01 R_\odot$, $R_2 = 1.14 \pm 0.01 R_\odot$, $L_1 = 0.52 \pm 0.01 L_\odot$, $L_2 = 1.34 \pm 0.01 L_\odot$, and $a = 2.32 \pm 0.01 R_\odot$ (here a is the separation between two components). The evolutionary status for this binary is plotted in the Hertzsprung–Russell (H–R) diagram (Fig. 4, solid symbols), which implies that the secondary star is still a main sequence star while the primary star has evolved away from the main sequence stage, indicating that the less massive but hotter primary star is more evolved than the secondary star.

The first orbital period investigations of IO Cnc are given in this paper. Based on the analyses of the $(O - C)$ curves, a sinusoidal variation, superimposed on a

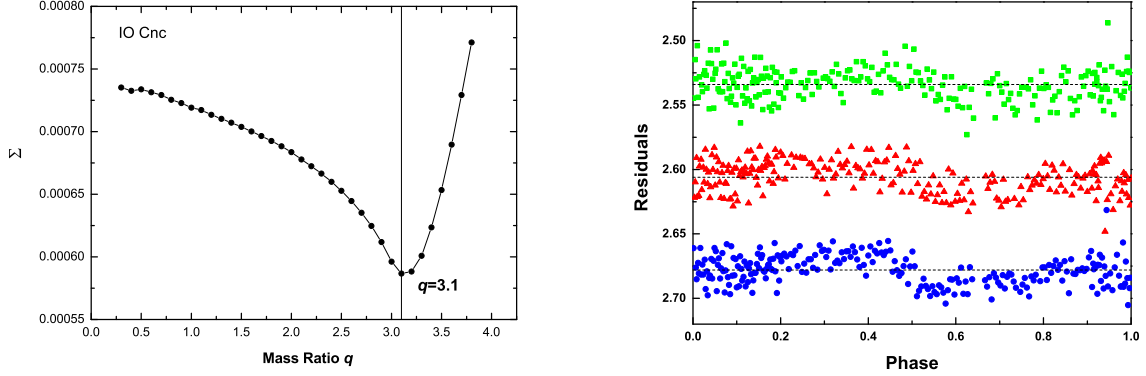


Fig. 2 Left panel: the q -search diagram of IO Cnc. The lowest point derived at $q = 3.1$. Right panel: residuals (observed minus calculated light curves) from the solutions.

Table 5 Photometric Solutions of IO Cnc

Parameters	Values	Values
	Basic solutions	with third light
Primary temperature T_1 (K)	5941 ± 83	5947 ± 10
Secondary temperature T_2^a (K)	5848 ± 38	5848 ± 38
Orbital inclination i ($^\circ$)	81.2 ± 0.2	81.7 ± 0.5
Mass ratio q (M_2/M_1)	3.120 ± 0.025	3.00 ± 0.10
Modified dimensionless surface potential ($\Omega_1 = \Omega_2$)	6.675 ± 0.031	6.51 ± 0.14
Luminosity ratio $L_{1V}/(L_{1V} + L_{2V})$	0.279 ± 0.001	0.2876 ± 0.0013
Luminosity ratio $L_{1R_c}/(L_{1R_c} + L_{2R_c})$	0.277 ± 0.001	0.2850 ± 0.0013
Luminosity ratio $L_{1I_c}/(L_{1I_c} + L_{2I_c})$	0.275 ± 0.001	0.2830 ± 0.0013
Luminosity ratio $L_3/(L_1 + L_2 + L_3)$ in band V	-	0.020 ± 0.021
Luminosity ratio $L_3/(L_1 + L_2 + L_3)$ in band R_c	-	0.019 ± 0.021
Luminosity ratio $L_3/(L_1 + L_2 + L_3)$ in band I_c	-	0.040 ± 0.020
Radius of star 1 (relative to semimajor axis) in pole direction r_1 (pole)	0.27287 ± 0.00065	0.2775 ± 0.0032
Radius of star 1 (relative to semimajor axis) in side direction r_1 (side)	0.28516 ± 0.00073	0.2901 ± 0.0035
Radius of star 1 (relative to semimajor axis) in back direction r_1 (back)	0.3233 ± 0.0010	0.3290 ± 0.0041
Radius of star 2 (relative to semimajor axis) in pole direction r_2 (pole)	0.4571 ± 0.0025	0.451 ± 0.011
Radius of star 2 (relative to semimajor axis) in side direction r_2 (side)	0.4922 ± 0.0035	0.485 ± 0.016
Radius of star 2 (relative to semimajor axis) in back direction r_2 (back)	0.5200 ± 0.0047	0.512 ± 0.021
Fillout factor f (%)	16.1 ± 5.0	18 ± 23
Equal-volume radius of star 1 (relative to semimajor axis) r_1	0.29545 ± 0.00047	0.2997 ± 0.0021
Equal-volume radius of star 2 (relative to semimajor axis) r_2	0.4911 ± 0.0021	0.4886 ± 0.0094

^aThe temperature is taken as the average of the T_{eff} in Qian et al. (2017).

continuous period change was derived. This pattern of orbital period changes also appears in many other shallow contact binaries (e.g., Qian et al. 2013a,b; Yang et al. 2008, 2009, 2010; Li et al. 2015a; Li et al. 2015b). For late-type binary IO Cnc, the cyclic variation may be interpreted as due to the magnetic activity of one or both components (Applegate 1992). With the following equations given by Rovithis-Livaniou et al. (2000) and Lanza & Rodonò (2002), respectively:

$$\Delta P = \sqrt{2[1 - \cos(2\pi P/P_3)]} \times A$$

and

$$\frac{\Delta P}{P} = -9 \frac{\Delta Q}{Ma^2}, \quad (3)$$

the required variation of the quadruple moment ΔQ can be calculated to be $\Delta Q_1 = 2.0 \times 10^{47}$ g cm² and $\Delta Q_2 = 6.2 \times 10^{47}$ g cm² for both components, respectively.

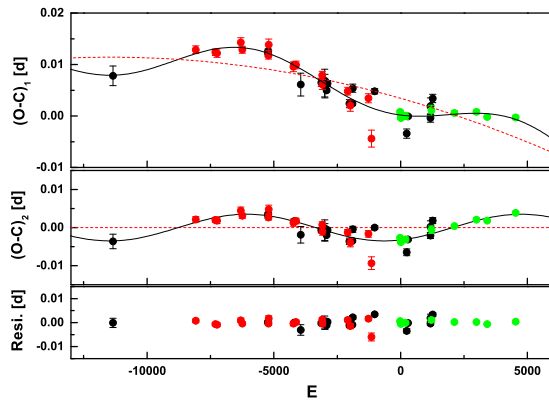
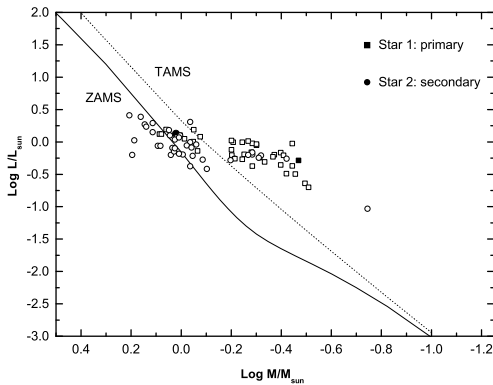
Assuming conservation of the orbital angular momentum, ΔQ for the close binary is on the order of $10^{51} - 10^{52}$ g cm² (Lanza & Rodonò 1999). Thus, the values of ΔQ_1 and ΔQ_2 for IO Cnc are too small, suggesting that the mechanism of Applegate cannot interpret the cyclic period variation of IO Cnc.

The statistical investigations given by Liao & Qian (2010) have shown that the most plausible mechanism causes the cyclic changes of the ($O - C$) diagrams is light travel time effect (LTTE) via the presence of a potential third body. Therefore, the cyclic variation was analyzed for LTTE. We use the following well-known equation

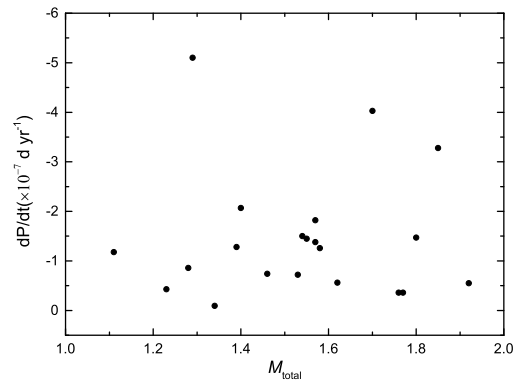
$$f(m) = \frac{(M_3 \sin i_3)^3}{(M_1 + M_2 + M_3)^2} = \frac{4\pi^2}{GP_3^2} \times (a_{12} \sin i_3)^3, \quad (4)$$

Table 6 Fitted Parameters of Orbital Period Variations (upper) and Orbital Parameters of the Tertiary Body (lower) for IO Cnc

Parameters	Values
Revised epoch, JD_0 (HJD)	$2456665.37687 \pm 0.00021$
Revised period, P_0 (d)	0.3476926 ± 0.0000002
Rate of the linear decrease, β (d yr $^{-1}$)	$(-1.28 \pm 0.43) \times 10^{-7}$
LTTE semi-amplitude, A (d)	0.0035 ± 0.0004
Orbital period, P_3 (yr)	10.29 ± 0.91
Initial phase, φ (degree)	-68.13 ± 0.12
Projected semi-major axis, $a_{12} \sin i_3$ (AU)	0.61 ± 0.07
Mass function, $f(m)$ (M_\odot)	0.002 ± 0.001
Mass, $M_{3\min}$ (M_\odot)	0.17 ± 0.02
Orbital semi-major axis, $a_{3\max}$ (AU)	4.88 ± 0.82

**Fig. 3** The $(O - C)$ diagram of IO Cnc. *Black dots* represent data collected from literature, *green and red dots* represent new observations in the present paper and times of light minima obtained from the CRTS project data, respectively. The lower panel shows residuals from the whole fitting effect.**Fig. 4** The H-R diagram.

to calculate orbital parameters of the tertiary body and the results are displayed in the bottom part of Table 6. The minima mass of the tertiary component ($i_3 = 90^\circ$) is

**Fig. 5** The relation between the total mass versus dp/dt for samples with period decreasing.

estimated as $M_{3\min} = 0.17 \pm 0.02 M_\odot$, and an orbital semi-major axis shorter than 4.88 ± 0.82 AU was obtained.

The contribution of the third light to the total system would then be roughly estimated to be $0.2 \pm 0.1\%$ with the relation of $L \sim M^{3.37}$ (Kippenhahn et al. 2012). Considering a potential third body in system, we tried to make l_3 as an adjustable parameter. Photometric solutions with a third light are close to the basic solutions, and the parameter errors are generally larger. We listed them in Column (3) of Table 5. The third light contributions are small: $2.0\% \pm 2.1\%$ in V , $1.9\% \pm 2.1\%$ in R_c , and $4.0\% \pm 2.0\%$ in I_c , which are close to the estimated value within the standard errors. This indicates that the orbital inclination of the third body in IO Cnc should be close to 90° . The fact that the third light contribution in I_c -band is the highest indicates that the third body may be a red dwarf. According to the parallax value of 0.83972 ± 0.06494 mas given by Gaia (Gaia Collaboration et al. 2018), the distance of the binary system is then 1190.87 ± 92.09 pc, therefore, the semi-major axis of the tertiary component corresponds to a small angular distance of $0''.004$. It seems difficult to detect this companion star under current measurement precision and detection capability.

Table 7 Some G-type Shallow Contact Binaries ($f \leq 20\%$)

Star	Period(d)	Sp. Type	$q(\text{or } l/q)$	M_{massive} (M_{\odot})	$i(^{\circ})$	$f(\%)$	Type	Eclipse	dp/dt ($\times 10^{-7} \text{ d yr}^{-1}$)	$T_3(\text{yr})$	Refs.
DE Lyn	0.4088188	G7	0.488	0.87	82.55	9.02	W	total	-5.1	-	H16
GV Leo	0.26673171	G7	0.1879	-	76.13	17.74	A	total	-4.95	-	^b , K13
SS Ari	0.40599	G0	0.308	1.3	77.306	9.4	W	partial	-4.03	37.75	L09
IK Boo	0.3031170	G2	0.873	0.986	61.3	2.22	W	partial	-3.28	9.74	K17
BX Peg	0.28042	G4.5	0.376	1.02	87.7	14.6	W	total	-2.07	57.8	L15a
AH Tau	0.332672375	G1	0.505	1.04	83.65	6.6	A	total	-1.823	54.62	X15a
V508 Oph	0.34479141	G0	0.52	1.01	83.78	15.4	A	total	-1.502	24.27	X15c
AQ Boo	0.333139	G0	0.455	1.24	71.9	14.43	W	partial	-1.47	-	W16
VW Boo	0.34232	G5	0.428	1.084	73.81	10.8	W	partial	-1.45	25.96	L11b
AU Ser	0.38498	G4	0.709	0.895	82.818	19.8	A	partial	-1.38	94.15	G05, P09, L11a
IO Cnc	0.347694	G0	0.320	1.05	81.10	16	W	total	-1.28	10.29	This study
AO Cam	0.32991	G0	0.413	1.119	76.0	12	W	partial	-1.26	7.63	Y10, B04
LO Com	0.2863621	G7	0.404	0.79	79.991	3.2	W	partial	-1.18	-	^b , Z16
V396 Mon	0.39634498	G2	0.392	0.92	89.7	18.9	W	total	-0.857	42.4	^b , L11a
TU Boo	0.32428	G3	0.508	0.97	88.9	16.5	A	total	-0.74	54.5	L07
U Peg	0.37478	G2	0.331	1.149(9)	77.51	15	A	partial	-0.72	19	P02
V524 Mon	0.28361714	G5	0.476	1.1	80.469	7.7	W	total	-0.56	23.93	H12
V417 Aql	0.37031480	G0	0.368	1.4	85.5	20.0	W	partial	-0.55	42.4	Q03a, L04
RW Com	0.23734706	G9	0.34	0.92	75.2	17	W	partial	-0.43	13.7	^b , M87, Y03
TY Boo	0.31715	G3	0.465	1.21	76.47	7.6	W	partial	-0.36	58.9	C12
EQ Tau	0.341348	G2	0.442	1.22	86.5	11.8	A	total	-0.36	22.7	L14
RW Dor	0.2857	G4/5	0.63	0.82	76.32	20	W	partial	-0.093	95.38	S11, S19
GQ Boo	0.384639624	G2	0.512	1.01(15)	62.86	14	W	partial	Y	-	Z17
TY UMa	0.35454813	G1	0.396	1.57(14)	84.9	13.4	W	total	+5.18	51.7 and 10	^b , L15c
DD Com	0.26920811	G7	0.272	-	74.4	8.7	W	partial	+3.4	-	Z10
AR Boo	0.344874	G9	0.388	0.90	77.2	12.5	W	partial	+2.77	7.57	L09a
CW Scl	0.3855865917	G0	0.39	-	86	7	A	total	+2.16	-	S16b
DD Indi	0.362746	G5	0.4528	-	85.9	11	W	total	+1.21	-	S16a
DF Hya	0.3305978	G3	0.424	1.02	84.3	12	W	total	+1.11	21.5	^b , N92, X09
V829 Her	0.3581	G2	0.435	1.30(3)	57.2	20	W	partial	+0.81	12.61	Y05, E06
UX Eri	0.44528226	G7	0.373	1.45	75.32	2.9	W	partial	+0.77	45.3	^b , Q07
YY Eri	0.3210	G3	0.44	1.54	82.12	10	W	total	+0.639	38.6 and 22.4	Y05, Y18
AE Phe	0.36237459	G0	0.45	1.38	86.45	14.6	W	total	+0.617	-	H09b, G76, Y05
AA UMa	0.46812501	G0	0.5525	1.61(3)	80.42	14.6	W	partial	+0.468	28.2	L11
V700 Cyg	0.340048	G2	0.5437	0.92	84.05	15.1	W	partial	+0.33	54.0	Y09
AW Vir	0.35399695	G3-G7	0.697	1.11	80.6	4.9	W	partial	+0.14	-	^b , H09a, Q03b
GSC 1537-1557	0.318275	G4	0.378	0.95	83.207	8.10	W	total	0	8.1	X15b
DF CVn	0.3268956	G7	0.28	0.63	68.55	20	A	partial	0	17.2	^b , D11
V737 Per	0.366599	G5:	0.41	1.20(4)	78.60	8.73	A	partial	0	0	H18
GW Cep	0.31883212	G3	0.3861	1.06	85.4	17.6	W	total	0	32.63	L10, Q03b
HH Boo	0.318618	G2	0.587	1.068	69.084	12.86	W	partial	0	6.58	H19
HO Psc	0.32469898	G7	0.436	0.91	79.98	7.9	W	partial	-	-	S12
MT Cam	0.36613937	G2	0.3385	-	83.5	13	W	total	-	-	^b , F18
V0951 Per	0.2704755	G8	0.658	-	76.56	12	A	partial	-	-	^b , K18
HL Lyn	0.2921654	G7	0.502	-	77.6	18.6	A	partial	-	-	^b , K18
CSS J075135.6+382028	0.3525725	G7	0.82	-	89.6	15	A	total	-	-	^b , K18
CSS J062803.2+571604	0.3224327	G7	0.893	-	57.0	11.8	A	partial	-	-	^b , K18
CSS J075350.1+264830	0.2606906	G9	0.450	-	86.42	18	W	total	-	-	^b , K18
EH Hya	0.2969	G7:	0.314	-	81.9	12	W	total	-	-	S91
TW Cet	0.3169	G5	0.575	1.06	85.7	3	W	total	-	-	Y05, A59

^bThe spectral types are taken from Qian et al. (2017).

References in alphabetical order: (A59) Archer (1959); (B04) Baran et al. (2004); (C12) Christopoulou et al. (2012); (D11a) Deb & Singh (2011); (D11b) Dai et al. (2011); (E06) Erdem & Özkardeş (2006); (F18) Faulkner et al. (2018); (G76) Grønbech (1976); (G05) Gürol (2005); (H09a) He & Qian (2009); (H09b) He et al. (2009); (H12) He et al. (2012); (H19) He & Wang (2019); (H16) Hashimoto et al. (2016); (H18) Hu et al. (2018); (K13) Kriwattanawong & Poojon (2013); (K17) Kriwattanawong et al. (2017); (K18) Kjurkchieva et al. (2018); (L04) Lee et al. (2004); (L07) Lee et al. (2007); (L09) Liu et al. (2009); (L09a) Lee et al. (2009); (L10) Lee et al. (2010); (L11) Lee et al. (2011); (L11a) Liu et al. (2011a); (L11b) Liu et al. (2011b); (L14) Li et al. (2014); (L15a) Li et al. (2015a); (L15c) Li et al. (2015c); (M87) Milone et al. (1987); (N92) Niarchos et al. (1992); (P02) Pribulla & Vanko (2002); (P09) Pribulla et al. (2009); (Q03a) Qian (2003a); (Q03b) Qian (2003b); (Q07) Qian et al. (2007); (S91) Samec et al. (1991); (S12) Samec et al. (2012); (S16a) Samec et al. (2016a); (S16b) Samec et al. (2016b); (S19) Sarotsakulchai et al. (2019); (W16) Wang et al. (2016); (X09) Xiang et al. (2009); (X15a) Xiang et al. (2015a); (X15b) Xiang et al. (2015b); (X15c) Xiang et al. (2015c); (Y03) Yang & Liu (2003); (Y05) Yakut & Eggleton (2005); (Y09) Yang & Dai (2009); (Y10) Yang et al. (2010); (Y18) Yu et al. (2018); (Z10) Zhu et al. (2010); (Z16) Zhang et al. (2016); (Z17) Zhang et al. (2017).

A sample of 50 G-type shallow contact binaries ($f \leq 20\%$ (Qian et al. 2013b)) were tabulated in Table 7 in descending order by period decrease/increase rate (dp/dt), where parameters include orbital period, spectral type, mass ratio (for W-type systems, the mass ratio values are listed as $1/q$), mass of the more massive component, orbital inclination, fill-out factor, subtype of WUMa-type eclipsing binary system, type of eclipse, long-term period change rate and oscillation period of ($O - C$) (where a horizontal line (-) indicates that it was not reported, “Y” indicates a long-term decrease period change exists in GQ Boo). The last nine stars needed more observation and orbital period analysis in future.

As shown in this table, most of the G-type shallow contact binaries are undergoing a long-term and periodic orbital period changes, and there are more systems showing long-term decreases. Recently studied object FV CVn (Liao & Sarotsakulchai 2019) and IO Cnc are both solar-type W-subtype contact binaries. FV CVn is a contact binary with pure periodic orbital period changes, while IO Cnc belongs to shallow contact configuration undergoing a long-term and periodic orbital period change. They are in different evolutionary states. The evolutionary statuses of these G-type shallow contact binaries are displayed in Figure 4 (open symbols), where the values of M and L are collected from Refs. in Table 7, or calculated with AbsParEB software (Liakos 2015) by inputting photometric solutions given in the corresponding Refs. As one can see from Table 7 and Figure 4, IO Cnc is a typical G-type shallow contact binary.

We attempt to discuss the relation between the total mass versus dp/dt for samples with period decreasing. As shown in Figure 5, there is no obvious relationship at present. Therefore, the long-term orbital period decreases with a rate of $(-1.28 \pm 0.43) \times 10^{-7} \text{ d yr}^{-1}$ for IO Cnc could be plausibly explained by the mass transfer from the more massive component to the less massive one rather than the angular momentum loss via magnetic braking. It is worth mentioning that photometric and spectrometric data on contact binaries have been accumulating rapidly owing to the large sky survey projects. Considering the increasing number of sample stars in future, the current statistical results of $M_{\text{total}} - dp/dt$ diagram may be inconclusive. Both the shallow contact configuration and the long-term period decrease may suggest that IO Cnc is a newly formed contact binary. Yang et al. (2007, 2009, 2010) studied orbital period changes and evolutionary status for the shallow contact binaries and, according to their conclusions, this kind of shallow contact binary with a decreasing period will evolve into a deep contact configuration.

Acknowledgements This work is supported by the National Natural Science Foundation of China (Grant Nos. 11873017 and 11933008), the Science and Technology Talents and Platform Plan of Yunnan province (2018HB070) and the Yunnan Natural Science Foundation (No. 2018FB006). New CCD observations were obtained with the 1 m and 60 cm telescopes at Yunnan Observatories. We also acknowledge the support of the staff of the Xinglong 85 cm telescope. This work was partially supported by the Open Project Program of the Key Laboratory of Optical Astronomy, National Astronomical Observatories, Chinese Academy of Sciences.

References

- Applegate, J. H. 1992, ApJ, 385, 621
 Archer, S. 1959, ApJ, 130, 774
 Baran, A., Zola, S., Rucinski, S. M., et al. 2004, Acta Astronomica, 54, 195
 Christopoulou, P. E., Papageorgiou, A., Vasileiadis, T., & Tsantilas, S. 2012, AJ, 144, 149
 Dai, H. F., Yang, Y. G., & Yin, X. G. 2011, New Astron., 16, 173
 Deb, S., & Singh, H. 2011, MNRAS, 412, 1787
 Diethelm, R. 2009, Information Bulletin on Variable Stars, 5894, 1
 Diethelm, R. 2010, Information Bulletin on Variable Stars, 5945, 1
 Diethelm, R. 2011, Information Bulletin on Variable Stars, 5992, 1
 Diethelm, R. 2012, Information Bulletin on Variable Stars, 6029, 1
 Diethelm, R. 2013, Information Bulletin on Variable Stars, 6063, 1
 Drake, A. J., Djorgovski, S. G., Mahabal, A., et al. 2009, ApJ, 696, 870
 Erdem, A., & Özkardeş, B. 2006, NewA, 12, 192
 Faulkner, D. R., Samec, R. G., & Caton, D. B. 2018, in American Astronomical Society Meeting Abstracts, 232, 317.11
 Gaia Collaboration, Brown, A. G. A., Vallenari, A., Prusti, T., et al. 2018, A&A, 616A, 1G
 Grønbech, B. 1976, A&AS, 24, 399
 Gürol, B. 2005, New Astron., 10, 653
 Hashimoto, A., Zhang, L., Han, X. L., et al. 2016, New Astron., 45, 77
 He, J. J., & Qian, S. B. 2009, in Astronomical Society of the Pacific Conference Series, 404, The Eighth Pacific Rim Conference on Stellar Astrophysics: A Tribute to Kam-Ching Leung, eds. S. J. Murphy, & M. S. Bessell, 194
 He, J. J., Qian, S. B., Fernández Lajús, E., & Fariña, C. 2009, AJ, 138, 1465
 He, J.-j., & Wang, J.-j. 2019, Advances in Astronomy, 2019, 5641518
 He, J.-J., Wang, J.-J., & Qian, S.-B. 2012, PASJ, 64, 85
 Hoňková, K., Juryšek, J., Lehký, M., et al. 2013, OEJV, 160, 1

- Hoňková, K., Juryšek, J., Lehký, M., et al. 2015, *OEJV*, 168, 1
- Hu, K., Cai, J.-T., Yu, Y.-X., & Xiang, F.-Y. 2018, *New Astron.*, 65, 52
- Hubscher, J., Lehmann, P. B., & Walter, F. 2012, *Information Bulletin on Variable Stars*, 6010, 1
- Hubscher, J. 2015, *Information Bulletin on Variable Stars*, 6152, 1
- Hubscher, J., & Monninger, G. 2011, *Information Bulletin on Variable Stars*, 5959, 1
- Juryšek, J., Hoňková, K., Šmelcer, L., et al. 2017, *OEJV*, 179, 1
- Kippenhahn, R., Weigert, A., & Weiss, A. 2012, *Stellar Structure and Evolution*
- Kjurkchieva, D. P., Popov, V. A., Vasileva, D. L., & Petrov, N. I. 2018, *New Astron.*, 62, 46
- Kriwattanawong, W., & Poojon, P. 2013, *RAA (Research in Astronomy and Astrophysics)*, 13, 1330
- Kriwattanawong, W., Sanguansak, N., & Maungkorn, S. 2017, *PASJ*, 69, 62
- Lanza A. F., & Rodonò M. 1999, *A&A*, 349, 887
- Lanza A. F., & Rodonò M. 2002, *AN*, 323, 424
- Lee, J.-W., Kim, C.-H., Lee, C.-U., & Oh, K.-D. 2004, *Journal of Astronomy and Space Sciences*, 21, 73
- Lee, J. W., Kim, H.-I., & Kim, S.-L. 2007, *PASP*, 119, 1099
- Lee, J. W., Lee, C.-U., Kim, S.-L., et al. 2011, *PASP*, 123, 34
- Lee, J. W., Youn, J.-H., Han, W., et al. 2010, *AJ*, 139, 898
- Lee, J. W., Youn, J.-H., Lee, C.-U., et al. 2009, *AJ*, 138, 478
- Li, K., Hu, S., Guo, D., et al. 2015a, *New Astron.*, 41, 17
- Li, K., Hu, S.-M., Guo, D.-F., et al. 2015b, *New Astron.*, 34, 217
- Li, K., Hu, S. M., Guo, D. F., et al. 2015c, *AJ*, 149, 120
- Li, K., Qian, S. B., Hu, S. M., & He, J. J. 2014, *AJ*, 147, 98
- Li, K., Xia, Q. Q., Hu, S. M., Guo, D. F., & Chen, X. 2018b, *PASP*, 130, 074201
- Li, L. J., & Qian, S. B. 2014, *MNRAS*, 444, 600
- Li, L. J., Qian, S. B., & Zhu, L. Y. 2018a, *ApJ*, 863, 151
- Liakos, A. 2015, in *Astronomical Society of the Pacific Conference Series*, 496, *Living Together: Planets, Host Stars and Binaries*, eds. S. M. Rucinski, G. Torres, & M. Zejda, 286
- Liao, W. P., & Qian, S. B. 2010, *MNRAS*, 405, 1930
- Liao, W. P., Qian, S. B., Li, K., et al. 2013, *AJ*, 146, 79
- Liao, W. P., Qian, S. B., & Sarotsakulchai, T. 2019, *AJ*, 157, 207
- Liao, W. P., & Sarotsakulchai, T. 2019, *PASP*, 131, 014202
- Liu, L., Qian, S. B., He, J. J., Zhang, J., & Li, L. J. 2009, *Ap&SS*, 321, 19
- Liu, L., Qian, S. B., Liao, W. P., et al. 2011a, *AJ*, 141, 44
- Liu, L., Qian, S. B., Zhu, L. Y., He, J. J., & Li, L. J. 2011b, *AJ*, 141, 147
- Milone, E. F., Wilson, R. E., & Hrivnak, B. J. 1987, *ApJ*, 319, 325
- Niarchos, M., Hoffmann, M., & Duerbeck, H. W. 1992, *A&A*, 258, 323
- Pribulla, T., & Vanko, M. 2002, *Contributions of the Astronomical Observatory Skalnaté Pleso*, 32, 79
- Pribulla, T., Rucinski, S. M., DeBond, H., et al. 2009, *AJ*, 137, 3646
- Qian, S. 2003a, *A&A*, 400, 649
- Qian, S. 2003b, *MNRAS*, 342, 1260
- Qian, S.-B., He, J.-J., Zhang, J., et al. 2017, *RAA (Research in Astronomy and Astrophysics)*, 17, 087
- Qian, S. B., Yuan, J. Z., Xiang, F. Y., et al. 2007, *AJ*, 134, 1769
- Qian, S. B., Liu, N. P., Liao, W. P., et al. 2013b, *AJ*, 146, 38
- Qian, S. B., Liu, N. P., Li, K., et al. 2013a, *ApJS*, 209, 13
- Rinner, C., Starkey, D., Demeautis, C., et al. 2003, *Information Bulletin on Variable Stars*, 5428, 1
- Rovithis-Livaniou, H., Kranidiotis, A. N., Rovithis, P., et al. 2000, *A&A*, 354, 904
- Samec, R. G., Charlesworth, S. D., & Dewitt, J. R. 1991, *AJ*, 102, 688
- Samec, R. G., Norris, C. L., Van Hamme, W., Faulkner, D. R., & Hill, R. L. 2016a, *AJ*, 152, 219
- Samec, R. G., Norris, C., Van Hamme, W. V., et al. 2016b, in *American Astronomical Society Meeting Abstracts*, 227, 437.07
- Samec, R. G., Smith, P. M., Robb, R., Faulkner, D. R., & Van Hamme, W. 2012, *PASP*, 124, 693
- Sarotsakulchai, T., Qian, S.-B., Soonthornthum, B., et al. 2019, *PASJ*, 71, 34
- Shi, X.-D., Qian, S.-B., Li, L.-J., Na, W.-W., & Zhou, X. 2020, *RAA (Research in Astronomy and Astrophysics)*, 20, 096
- Terrell, D., & Wilson, R. E. 2005, *Ap&SS*, 296, 221
- Van Hamme, W., & Wilson, R. E. 2007, *ApJ*, 661, 1129
- Wang, J.-J., He, J.-J., & Zhao, S.-Q. 2020, *RAA (Research in Astronomy and Astrophysics)*, 20, 050
- Wang, J. J., Jiang, L. Q., Zhang, B., Zhao, S. Q., & Yu, J. 2017, *PASP*, 129, 124202
- Wang, S., Zhang, L., Pi, Q., et al. 2016, *New Astron.*, 48, 42
- Wilson, R. E. 2012, *AJ*, 144, 73
- Wilson, R. E., & Devinney, E. J. 1971, *ApJ*, 166, 605
- Xiang, F., Xie, W., Tian, Y., & Tao, X. 2009, *PASJ*, 61, 707
- Xiang, F.-Y., Xiao, T.-Y., & Yu, Y.-X. 2015a, *AJ*, 150, 25
- Xiang, F. Y., Xiao, T. Y., Zhang, B., & Shi, X. D. 2015b, *AJ*, 150, 9
- Xiang, F.-Y., Yu, Y.-X., & Xiao, T.-Y. 2015c, *AJ*, 149, 62
- Yakut, K., & Eggleton, P. P. 2005, *ApJ*, 629, 1055
- Yang, Y.-G., & Dai, H.-F. 2009, *PASJ*, 61, 577
- Yang, Y. G., Dai, J. M., Yin, X. G., & Xiang, F. Y. 2007, *AJ*, 134, 179
- Yang, Y. G., Lü, G. L., Yin, X. G., et al. 2009, *AJ*, 137, 236
- Yang, Y. G., Wei, J. Y., & He, J. J. 2008, *AJ*, 136, 594
- Yang, Y. G., Wei, J. Y., Kreiner, J. M., & Li, H. L. 2010, *AJ*, 139, 195
- Yang, Y., & Liu, Q. 2003, *PASP*, 115, 748
- Yu, T., Hu, K., Yu, Y.-X., & Xiang, F.-Y. 2018, *RAA (Research in Astronomy and Astrophysics)*, 18, 106
- Zhang, B., Qian, S.-B., Wang, J.-J., et al. 2020, *RAA (Research in Astronomy and Astrophysics)*, 20, 047
- Zhang, J., Qian, S.-B., Han, Z.-T., & Wu, Y. 2017, *MNRAS*, 466, 1118
- Zhang, Y., Han, Q. W., & Liu, J. Z. 2016, *PASP*, 128, 124201
- Zhou, X., & Soonthornthum, B. 2020, *RAA (Research in Astronomy and Astrophysics)*, 20, 010
- Zhu, L., Qian, S. B., Mikulášek, Z., et al. 2010, *AJ*, 140, 215